

# Analyses of protein cores reveal fundamental differences between solution and crystal structures

Zhe Mei<sup>1,2</sup>, John D. Treado<sup>1,3</sup>, Alex T. Grigas<sup>1,4</sup>, Zachary A. Levine<sup>5,6</sup>, Lynne Regan<sup>7</sup>, and Corey S. O’Hern<sup>1,3,4,8,9</sup>

<sup>1</sup>Integrated Graduate Program in Physical & Engineering Biology, Yale University, New Haven, Connecticut 06520, USA

<sup>2</sup>Department of Chemistry, Yale University, New Haven, Connecticut 06520, USA

<sup>3</sup>Department of Mechanical Engineering & Materials Science, Yale University, New Haven, Connecticut 06520, USA

<sup>4</sup>Graduate Program in Computational Biology & Bioinformatics, Yale University, New Haven, Connecticut 06520 USA

<sup>5</sup>Department of Pathology, Yale University, New Haven, Connecticut 06520, USA

<sup>6</sup>Department of Molecular Biophysics and Biochemistry, Yale University, New Haven, Connecticut, 06520

<sup>7</sup>Institute of Quantitative Biology, Biochemistry and Biotechnology, Center for Synthetic and Systems Biology, School of Biological Sciences, University of Edinburgh

<sup>8</sup>Department of Physics, Yale University, New Haven, Connecticut 06520, USA

<sup>9</sup>Department of Applied Physics, Yale University, New Haven, Connecticut 06520, USA

November 18, 2021

## Abstract

There have been several studies suggesting that protein structures solved by NMR spectroscopy and x-ray crystallography show significant differences. To understand the origin of these differences, we assembled a database of high-quality protein structures solved by both methods. We also find significant differences between NMR and crystal structures—in the root-mean-square deviations of the C<sub>α</sub> atomic positions, identities of core amino acids, backbone and sidechain dihedral angles, and packing fraction of core residues. In contrast to prior studies, we identify the physical basis for these differences by modelling protein cores as jammed packings of amino-acid-shaped particles. We find that we can tune the jammed packing fraction by varying the degree of thermalization used to generate the packings. For an athermal protocol, we find that the average jammed packing fraction is identical to that observed in the cores of protein structures solved by x-ray crystallography. In contrast, highly thermalized packing-generation protocols yield jammed packing fractions that are even higher than those observed in NMR structures. These results indicate that thermalized systems can pack more densely than athermal systems, which suggests a physical basis for the structural differences between protein structures solved by NMR and x-ray crystallography.

It is generally acknowledged that protein structures determined by x-ray crystallography versus NMR exhibit small but significant differences. It is by no means resolved, however, whether these differences stem from differences in the experimental methods themselves, or if they reflect physical differences in proteins under the different conditions in which the measurements are made [1, 3,

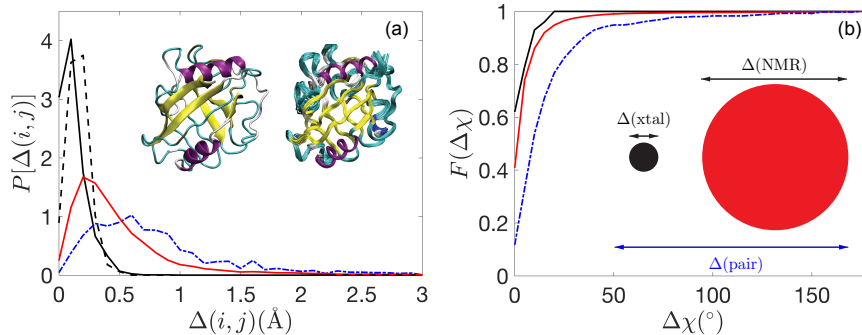


Figure 1: (a) Probability distributions  $P(\Delta(i, j))$  of the root-mean-square deviations (RMSD) in the positions of the  $C_\alpha$  atoms (in  $\text{\AA}$ ) for core residues in duplicate x-ray crystal structures (solid black line), in the NMR model ensemble for each structure (solid red line), and in paired x-ray crystal and NMR structures (dot-dashed blue line). We also plot the distribution for  $\Delta = \sqrt{3B/8\pi^2}$  from the B-factor for core  $C_\alpha$  atoms in the duplicate x-ray crystal structures (dashed black line). The inset shows an example of one of the proteins in the paired x-ray crystal and NMR structure dataset, with the x-ray crystal structure on the left and the bundle of 20 NMR structures on the right (PDB codes 3K0M and 1OCA, respectively). The  $\alpha$ -helices are colored purple, the  $\beta$ -sheets are yellow, and the loops are gray. (b) The fraction of core amino acids  $F(\Delta\chi)$  with root-mean-square deviations of the side chain dihedral angles less than  $\Delta\chi$  (in degrees) for the pairwise comparisons in (a). The inset is a schematic in two dimensions of the high-dimensional volume in configuration space that the  $C_\alpha$  atoms in core residues in x-ray crystal structures and NMR ensembles sample. X-ray crystal structures sample a smaller region than NMR ensembles, but the distance *between* these regions of configuration space is larger than the fluctuations of both the x-ray crystal and NMR structures. The relative lengths of the arrows are drawn to scale, with  $\langle\Delta\rangle \approx 0.1, 0.5, \text{ and } 0.8 \text{ \AA}$  for the x-ray duplicates, NMR models, and pairs of x-ray crystal and NMR structures, respectively.

8, 11, 12, 14, 15, 19]. To begin to answer this question, one must directly compare high-quality structures of the same protein solved by both methods. Choosing x-ray crystal structures based on their resolution is a straightforward way to identify well-specified structures. In our database of structures solved by both x-ray crystallography and NMR, we only include structures that have been solved by x-ray crystallography at a resolution of  $2\text{\AA}$  or less.

There is, however, no universally accepted metric to assess the quality of NMR structures. We therefore defined one. Specifically, we determined the number of NMR restraints per residue beyond which structures do not change significantly with the addition of more restraints, and only used structures with at least this number of restraints per residue on average. Applying these selection criteria, we created a data set of 16 proteins whose structures have been determined by both x-ray crystallography and NMR. We created an additional dataset of 51 high-quality NMR protein structures (defined in the same way), for which there is no companion x-ray crystal structure, in an attempt to exclude any influence of crystallizability on the NMR protein structures. In addition, as a reference set of high-resolution protein structures solved by x-ray crystallography, we use a dataset of 221 high-resolution protein structures collected by Wang and Dunbrack [17]. Finally, we created a dataset of structures that have been solved multiple times by x-ray crystallography, with resolution of  $2\text{\AA}$  or less and the same crystal forms and space groups, to allow us to assess structural variations that arise from thermal fluctuations.

We find that the root-mean-square deviations (RMSD) of the positions of core  $C_\alpha$  atoms within an NMR ‘bundle’ is greater than the RMSD of core  $C_\alpha$  atoms of the set of protein crystal structures

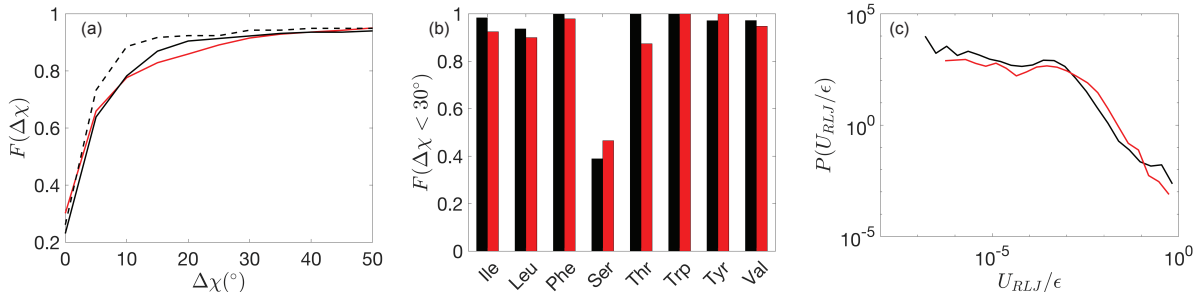


Figure 2: (a) Fraction of side chain conformations of core residues with predictions from the hard-sphere plus stereochemical constraint model that deviate from the experimentally observed values by less than  $\Delta\chi$  (in degrees) in the dataset of x-ray crystal (black line) and NMR (red line) structure pairs, and the Dunbrack 1.0 dataset of 221 high resolution x-ray crystal structures [17, 18]. (b) Fraction of core hydrophobic side chains, grouped by residue type, that can be predicted to within  $30^\circ$  of the corresponding experimental structure using the hard-sphere plus stereochemical constraint model for xray (black bars) and NMR structures (red bars). (c) Distribution of the overlap potential energy  $U_{RLJ}/\epsilon$ , calculated using Eq. (3) for core residues in the x-ray crystal (black line) and NMR structures (red line) in the paired dataset.

that have been solved multiple times. Also, the difference between an x-ray crystal structure and each structure in the NMR bundle is greater than the spread within the NMR bundle. To gain deeper insight into these differences, we first analyzed side chain repacking of core residues in structures determined by both NMR and x-ray crystallography, using the hard-sphere plus stereochemical constraint model for both. We have shown in previous work that the ability to accurately predict the placement of sidechains of core residues is correlated with the high packing fraction  $\langle\phi\rangle \approx 0.55$  found in protein cores. We are able to predict the placement of side chains of core residues to above 90% accuracy to within  $30^\circ$  in structures determined by either x-ray crystallography or NMR, which is indicative of dense packing. When we explicitly calculate the packing fraction of core residues in protein structures determined by x-ray crystallography versus NMR, we find that that the cores of NMR structures are more tightly packed than the cores of x-ray crystal structures.

To further explore the physical basis for these observations, we generated jammed packings of amino-acid-shaped particles computationally, and explored the extent to which we can tune their packing fraction using protocols with different degrees of thermalization. We find that depending on the thermalization protocol we use, we can match the packing fraction to that which we observe in structures determined by x-ray crystallography and by NMR. Specifically, the packing fraction of amino acid-shaped particles we observe in the athermal limit corresponds to the packing fraction we find in the cores of protein crystal structures, whereas the packing fraction we observe in the cores of structures determined by NMR is higher, but less than the packing fraction achieved from a high degree of thermalization. Thus, the core packing fraction we observe for protein structures determined by x-ray crystallography and NMR are both physically reasonable, and we speculate that the higher packing fraction we observe for structures determined by NMR reflects the different conditions under which NMR structures are determined.

We first compare pairs of structures, determined by x-ray crystallography and NMR, by quantifying the root-mean-square deviation (RMSD) of the  $C_\alpha$  positions of a given set of residues defined

by their sequence location on two structures  $i$  and  $j$ :

$$\Delta(i, j) = \sqrt{\frac{1}{N_S} \sum_{\mu=1}^{N_s} (\vec{c}_{\mu,j} - \vec{c}_{\mu,i})^2}, \quad (1)$$

where  $\vec{c}_{\mu,i}$  is the position of the  $C_\alpha$  atom on residue  $\mu$  in structure  $i$ , and  $N_S$  is the number of residues being compared. For the NMR datasets,  $i$  and  $j$  represent each model within a bundle and for the x-ray crystal duplicate dataset,  $i$  and  $j$  represent each of the duplicates. We define core residues as residues with small ( $< 10^{-3}$ ) relative solvent-accessible surface area (rSASA), as defined in Eq. (1) in the SI. In Fig. 1 (a), we compare the distributions  $P(\Delta(i, j))$  of RMSD values of core residues in x-ray crystal structure duplicates and RMSD values of core residues in NMR bundles. We show that the fluctuations among x-ray crystal structure duplicates are consistent with B-factor fluctuations of the  $C_\alpha$  positions of core residues, which are given by  $\Delta = \sqrt{3B/8\pi^2}$ . We also compare x-ray crystal and NMR structures for the same proteins by calculating the RMSD between  $C_\alpha$  atoms of core residues.

We also calculate the side chain dihedral angle fluctuations  $\Delta\chi$  for the same pairs of structures; we define  $\Delta\chi(\mu|i, j)$  as the distance between the sidechain conformations of residue  $\mu$  within structures  $i$  and  $j$ , i.e.

$$\Delta\chi(\mu|i, j) = \sqrt{(\vec{\chi}_{\mu,j} - \vec{\chi}_{\mu,i})^2}. \quad (2)$$

where  $\vec{\chi}_{\mu,i}$  is the set of dihedral angles  $(\chi_1, \dots, \chi_m)$  for residue  $\mu$  on structure  $i$ . Note that in Fig. 1(b), we measure  $\Delta\chi$  between two experimental structures of the same protein, whereas in Fig. 2 (a) and (b) we measure  $\Delta\chi$  between an experimental structure and a prediction using the hard-sphere plus stereochemical constraint model.

In Fig. 1, we show that the conformations of both the backbone and sidechains of core residues fluctuate less in x-ray crystal structures compared to the conformations within an NMR bundle, but that the fluctuations within an NMR bundle are smaller than those *between* the x-ray crystal and NMR structure pairs [3, 8, 15]. The inset to Fig. 1 (b) illustrates the proportion of configuration space sampled for structures solved by both NMR and x-ray crystallography. Structures determined by x-ray crystallography sample states in a relatively small volume of configuration space compared to that sampled by structures in an NMR bundle. Moreover, these two ensembles are separated by a characteristic distance that is larger than the scale of fluctuations in either ensemble.

To put these structural differences in context, we also analyze fluctuations in a database of pairs of x-ray crystal structures of wild-type proteins and the same protein with a single core mutation and also high-scoring submissions from a recent Critical Assessment of Protein Structure Prediction (CASP) competition [13]. We find that the scale of the fluctuations of single-site core mutants relative to wildtype structures is similar to that observed in x-ray crystal structure duplicates. In contrast, submissions to CASP12 exhibit much larger fluctuations. Because the CASP12 submissions are computational predictions, not experimentally determined structures, one would expect large structural fluctuations among the different CASP12 submissions. The scale of the structural fluctuations among the CASP12 submissions is also larger than those between structures of the same protein determined by x-ray crystallography or NMR. In the SI, we report additional measures of structural fluctuations, such as fluctuations in the identities of residues that make up the core.

To investigate the possible origin of the differences between structures determined by x-ray crystallography and NMR, we first investigated if these differences are due to the physical forces governing side chain placement in the core. In previous work, we showed that the hard-sphere plus stereochemical constraint model can uniquely specify the sidechain dihedral angles of hydrophobic

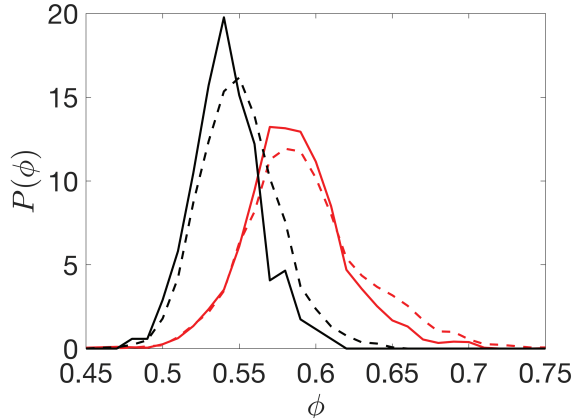


Figure 3: Distribution  $P(\phi)$  of the packing fraction of core residues in the Dunbrack 1.0 dataset of high-resolution x-ray crystal structures (black dashed line), the dataset of high-resolution NMR structures for which there is not a corresponding x-ray crystal structure (red dashed line), and x-ray crystal structures (black solid line) and NMR structures (red solid) from the paired dataset.

residues in the cores of protein crystal structures [2, 5, 7, 20]. One potential source of the differences in the fluctuations measured in NMR and crystal structure cores could be that the cores in NMR structures are less well-resolved, and the sidechains are poorly placed due to insufficient information to uniquely define their conformations. Such methodological inaccuracies have been suggested by previous studies, where computational refinement moves the NMR backbone and sidechain dihedral angles towards values similar to those of x-ray crystal structures [8, 11, 12, 14]. However, as shown in Fig. 2, we find that with our high-quality dataset of NMR structures we can repack hydrophobic side chains of core residues just as accurately as we can repack the same side chains in high-resolution x-ray crystal structures. The repacking protocol is outlined in detail in the SI, but briefly, we define the probability that a given residue  $\mu$  has adopted a given side chain conformation  $\vec{\chi}_\mu$  as  $P(\vec{\chi}_\mu) \propto \exp[-\beta U_{\text{RLJ}}(\vec{\chi}_\mu)]$ , where

$$U_{\text{RLJ}}(\vec{\chi}_\mu) = \sum_{\nu=1}^N \sum_{i,j} \frac{\epsilon}{72} \left[ 1 - \left( \frac{\sigma_{ij}^{\mu\nu}}{r_{ij}^{\mu\nu}} \right)^6 \right]^2 \Theta(\sigma_{ij}^{\mu\nu} - r_{ij}^{\mu\nu}) \quad (3)$$

is the purely repulsive Lennard-Jones potential energy of residue  $\mu$ , evaluated as a sum over all non-bonded atomic interactions.  $r_{ij}^{\mu\nu}$  is the distance between atoms  $i$  and  $j$  on residues  $\mu$  and  $\nu$ ,  $\sigma_{ij}^{\mu\nu} = (\sigma_i^\mu + \sigma_j^\nu)/2$ , and  $\sigma_i^\mu$  is the diameter of atom  $i$  on residue  $\mu$ .

However, when we investigate the packing fraction  $\phi$  of core residues for x-ray crystal and NMR structures, we find important differences. In Fig. 3, we plot the probability distribution  $P(\phi)$  of the packing fraction for core residues in x-ray crystal and NMR structures. The average packing fraction of core residues in the protein structures in the datasets determined by x-ray crystallography is  $\langle \phi \rangle = 0.55 \pm 0.01$ , a value that is consistent with our previous results for the packing fraction of core residues in globular and transmembrane protein cores and the cores of protein-protein interfaces solved by x-ray crystallography [7]. For core residues of protein structures in the NMR database, the average packing fraction is higher with  $\langle \phi \rangle = 0.59 \pm 0.02$ . We believe that this is the first time that such a difference in the packing fraction of core residues in high-quality protein structures determined by both x-ray crystallography and NMR has been reported.

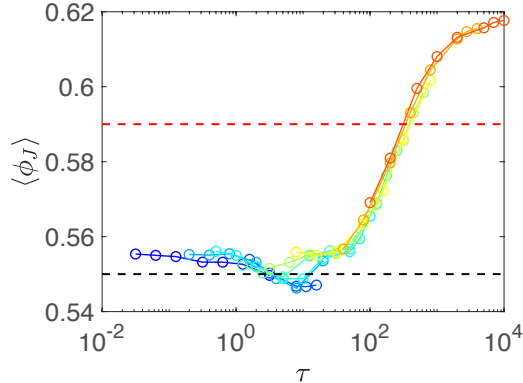


Figure 4: The ensemble-averaged packing fraction  $\langle \phi_J \rangle$  of jammed packings of amino-acid-shaped particles versus the dimensionless thermalization timescale  $\tau$  for a system with  $N = 16$  particles. Different colors represent simulations with different dimensionless temperatures  $k_B T / \epsilon$ , logarithmically spaced from  $10^{-7}$  (blue) to 1 (red). The dashed black line at  $\langle \phi_J \rangle = 0.55$  is the average packing fraction of core residues in x-ray crystal structures, and the dashed red line at  $\langle \phi_J \rangle = 0.59$  is the average packing fraction of core residues in NMR structures.

We were concerned that the higher packing fraction of core residues in protein structures determined by NMR could be an artifact, for example, the result of improperly-placed sidechains that overlap with neighboring residues, which would artificially increase the observed packing fraction. With this concern in mind, we calculated and compared the potential energy of atomic overlaps of non-bonded atoms  $U_{RLJ}$  for the structures determined by x-ray crystallography and NMR. However, we found that structures determined by either method have virtually identical overlap energies as shown in Fig. 2 (c), and we therefore ruled out this potential cause. The difference in the packing fraction of core residues was at first surprising, because our previous studies showed that the cores of x-ray crystal structures pack as densely as jammed packings of purely-repulsive amino-acid-shaped particles without backbone constraints generated using a protocol of successive compressions followed by energy minimization [6, 16].

We therefore revisited the protocol with which we prepared jammed packings of amino-acid-shaped particles [6, 16]. In our previous work, packings were prepared using an “athermal” protocol, where kinetic energy was drained rapidly from the system during the packing preparation. For the athermal protocol, amino acids were initialized in a cubic simulation box at a small initial packing fraction  $\phi_0$  and compressed by small increments  $\Delta\phi$  with each followed by energy minimization. (See SI for additional details.) Because the amino-acid-shaped particles were not allowed to translate and rotate significantly between each compression step, the jammed packings at  $\langle \phi \rangle \approx 0.55$  were obtained at the first metastable jammed state that the protocol encountered. Thus, the packing fractions that can be achieved by amino-acid-shaped particles is protocol-dependent. We therefore investigated more thermalized protocols to generate jammed packings of amino-acid-shaped particles.

We chose a family of quasi-annealing packing-generation protocols. We initialize the system in a dilute configuration, and compress the system in small increments  $\Delta\phi$  between periods of molecular dynamics simulations in the canonical ensemble for a time period  $t_{MD}$  at thermal energy  $k_B T$ . (See SI for details.) We find that temperature only acts to renormalize the simulation time window  $t_{MD}$ , i.e. a longer simulation run at a lower temperature will yield the same results as a shorter simulation run at a higher temperature. Thus, there is another time scale associated with

the quasi-annealing protocol,  $t_{\text{QA}} = c(T)t^*$ , where  $c(T)$  is a dimensionless quantity that depends on temperature,  $t^* = \sqrt{m_R\sigma_R^2/\epsilon}$ , and  $m_R$  and  $\sigma_R$  are the mass and diameter of the smallest residue. We find that plotting the packing fraction versus  $\tau$ , where

$$\tau = t_{\text{MD}}/t_{\text{QA}} = n \left( \frac{k_B T}{\epsilon} \right)^\alpha, \quad (4)$$

collapses the data for different temperatures and time periods onto a single curve as shown in Fig. 4. The exponent  $\alpha = 0.4 \pm 0.01$  and  $n$  is the number of time steps between compression increments.

Two limits of packing fractions emerge over the broad range of quasi-annealing protocols we tested; an athermal limit, which corresponds to packing fractions one finds in the cores of x-ray crystal structures [6, 7], and the completely thermalized limit, which can reach average packing fractions  $\langle\phi\rangle \approx 0.62$ . The packing fractions observed in the cores of protein structures solved by NMR fall between these two extremes with  $\langle\phi\rangle = 0.59$ . The states at exceedingly high packing fractions exist only in the limit of extremely long annealing times. The results of simulations using different protocols are consistent with the differences observed in the cores of protein structures solved by x-ray crystallography and NMR. The fact that thermalized packing protocols can yield NMR-like packing fractions, and that athermal protocols generate x-ray crystal-like packing fractions, suggests that native-state fluctuations are distinct for these two methods.

A previous study that also compared protein structures determined by x-ray crystallography and NMR suggested that the crystal environment restricts dynamical fluctuations, whereas bundles of NMR structures in solution contain the full dynamics one would expect from elastic network models for proteins [19]. The work we present here provides significant further evidence to support this conclusion, but whether the differences are due to crystalline contacts [9, 15, 19] or the different temperatures at which the protein structures are characterized [4, 10] remains to be determined.

## Author Contributions

Z.M. and J.D.T. contributed equally to this article. Z.M., J.D.T., Z.A.L., L.R., and C.S.O. designed the research. Z.M. compiled the dataset of protein structures, J.D.T. carried out simulations, and Z.M., J.D.T., Z.A.L., L.R. and C.S.O. interpreted the results. Z.M., J.D.T., C.S.O. and L.R. wrote the article.

## Acknowledgments

The authors acknowledge support from NIH training Grant No. T32EB019941 (J.D.T.), the Raymond and Beverly Sackler Institute for Biological, Physical, and Engineering Sciences (Z.M.), and NSF Grant No. PHY-1522467 (C.S.O.). This work also benefited from the facilities and staff of the Yale University Faculty of Arts and Sciences High Performance Computing Center. We thank Pat Loria and Peter Moore for helpful discussions.

## References

- [1] R. B. Best, K. Lindorff-Larsen, M. A. DePristo, and M. Vendruscolo. Relation between native ensembles and experimental structures of proteins. *Proceedings of the National Academy of Sciences*, 103(29):10901–10906, 2006. ISSN 0027-8424. doi: 10.1073/pnas.0511156103.

- [2] D. Caballero, A. Virrueta, C. O’Hern, and L. Regan. Steric interactions determine side-chain conformations in protein cores. *Protein Engineering, Design and Selection*, 29(9):367–376, 2016.
- [3] J. K. Everett, R. Tejero, S. B. K. Murthy, T. B. Acton, J. M. Aramini, M. C. Baran, J. Benach, J. R. Cort, A. Eletsy, F. Forouhar, R. Guan, A. P. Kuzin, H.-W. Lee, G. Liu, R. Mani, B. Mao, J. L. Mills, A. F. Montelione, K. Pederson, R. Powers, T. Ramelot, P. Rossi, J. Seetharaman, D. Snyder, G. V. T. Swapna, S. M. Vorobiev, Y. Wu, R. Xiao, Y. Yang, C. H. Arrowsmith, J. F. Hunt, M. A. Kennedy, J. H. Prestegard, T. Szyperski, L. Tong, and G. T. Montelione. A community resource of experimental data for nmr / x-ray crystal structure pairs. *Protein Science*, 25(1):30–45, 2016. doi: 10.1002/pro.2774.
- [4] J. S. Fraser, H. van den Bedem, A. J. Samelson, P. T. Lang, J. M. Holton, N. Echols, and T. Alber. Accessing protein conformational ensembles using room-temperature x-ray crystallography. *Proceedings of the National Academy of Sciences*, 108(39):16247–16252, 2011. ISSN 0027-8424. doi: 10.1073/pnas.1111325108.
- [5] J. Gaines, A. Virrueta, D. Buch, S. Fleishman, C. O’Hern, and L. Regan. Collective repacking reveals that the structures of protein cores are uniquely specified by steric repulsive interactions. *Protein Engineering, Design and Selection*, 30(5):387–394, 2017.
- [6] J. C. Gaines, W. W. Smith, L. Regan, and C. S. O’Hern. Random close packing in protein cores. *Phys. Rev. E*, 93:032415, 2016.
- [7] J. C. Gaines, S. Acebes, A. Virrueta, M. Butler, L. Regan, and C. S. O’Hern. Comparing side chain packing in soluble proteins, protein-protein interfaces and transmembrane proteins. *Proteins: Structure, Function, and Bioinformatics*, 86(5):581–591, 2018. doi: 10.1002/prot.25479.
- [8] S. O. Garbuzynskiy, B. S. Melnik, M. Y. Lobanov, A. V. Finkelstein, and O. V. Galzitskaya. Comparison of x-ray and nmr structures: Is there a systematic difference in residue contacts between x-ray- and nmr-resolved protein structures? *Proteins: Structure, Function, and Bioinformatics*, 60(1):139–147, 2005. doi: 10.1002/prot.20491.
- [9] B. Halle. Biomolecular cryocrystallography: Structural changes during flash-cooling. *Proceedings of the National Academy of Sciences*, 101(14):4793–4798, 2004. ISSN 0027-8424. doi: 10.1073/pnas.0308315101.
- [10] X. Hu, L. Hong, M. Dean Smith, T. Neusius, X. Cheng, and J. C. Smith. The dynamics of single protein molecules is non-equilibrium and self-similar over thirteen decades in time. *Nature Physics*, 12:171–174, 11 2015.
- [11] J. Koehler Leman, A. R. D’Avino, Y. Bhatnagar, and J. J. Gray. Comparison of nmr and crystal structures of membrane proteins and computational refinement to improve model quality. *Proteins: Structure, Function, and Bioinformatics*, 86(1):57–74, 2018. doi: 10.1002/prot.25402.
- [12] B. Mao, R. Tejero, D. Baker, and G. T. Montelione. Protein nmr structures refined with rosetta have higher accuracy relative to corresponding x-ray crystal structures. *Journal of the American Chemical Society*, 136(5):1893–1906, 02 2014. doi: 10.1021/ja409845w.



- [13] J. Moult, K. Fidelis, A. Kryshtafovych, T. Schwede, and A. Tramontano. Critical assessment of methods of protein structure prediction (casp)—round xii. *Proteins: Structure, Function, and Bioinformatics*, 86(S1):7–15, 2 2018. ISSN 1097-0134. doi: 10.1002/prot.25415.
- [14] M. Schneider, X. Fu, and A. E. Keating. X-ray vs. nmr structures as templates for computational protein design. *Proteins: Structure, Function, and Bioinformatics*, 77(1):97–110, 2009. doi: 10.1002/prot.22421.
- [15] K. Sikic, S. Tomic, and O. Carugo. Systematic comparison of crystal and nmr protein structures deposited in the protein data bank. *The Open Biochemistry Journal*, 4(83-95):83–95, 2010.
- [16] J. D. Treado, Z. Mei, L. Regan, and C. S. O’Hern. Void distributions reveal structural link between jammed packings and protein cores. *Phys. Rev. E*, 99:022416, 2019.
- [17] G. Wang and R. L. Dunbrack, Jr. PISCES: A protein sequence culling server. *Bioinformatics*, 19(12):1589–1591, 2003.
- [18] G. Wang and R. L. Dunbrack, Jr. PISCES: Recent improvements to a PDB sequence culling server. *Nucleic Acids Research*, 33:W94–8, 2005.
- [19] L.-W. Yang, E. Eyal, C. Chennubhotla, J. Jee, A. M. Gronenborn, and I. Bahar. Insights into equilibrium dynamics of proteins from comparison of nmr and x-ray data with computational predictions. *Structure*, 15(6):741 – 749, 2007. ISSN 0969-2126. doi: <https://doi.org/10.1016/j.str.2007.04.014>.
- [20] A. Q. Zhou, C. S. O’Hern, and L. Regan. Predicting the side-chain dihedral angle distributions of nonpolar, aromatic, and polar amino acids using hard sphere models. *Proteins: Structure, Function, and Bioinformatics*, 82(10):2574–2584, 2014.